Check for updates

Photoluminescence properties of a novel red fluoride K₂LiGaF₆:Mn⁴⁺ nanophosphor†

Yiwen Zhu,[a] Jinbo Yu,[a] Yong Liu,[a] Mikhail G. Brik,[bcd] Lin Huang,[a] Tongtong Xuan [iD][a] and Jing Wang [iD] *[a]

Red $K_2LiGaF_6:Mn^{4+}$ phosphors have been synthesized by the facile cation-exchange method. To optimize the optical properties, the phosphors were synthesized by using different reaction conditions. The highest luminescence intensity was increased 3.6 times for the Mn concentration of 1%, reaction temperature of 20 °C, and reaction time of 1 h. Replacement of the trivalent Al by Ga resulted in $K_2LiGaF_6:Mn^{4+}$ having better photoluminescence properties than $K_2LiAlF_6:Mn^{4+}$. Furthermore, the studies of the temperature-dependent emission intensity of the phosphors confirmed their good thermal stability, making them promising red phosphor candidates for white light-emitting diodes.

1. Introduction

White light-emitting diodes (LEDs) have attracted considerable attention as an energy-saving light source for a long time.[1–6] Commercial white LEDs fabricated by a blue LED chip with a yellow YAG:Ce³⁺ phosphor still suffer from some drawbacks such as low color rendering index (Ra < 80) and high correlated color temperature (CCT > 6000 K) because of the lack of a red light component.[7–9] So, great efforts have been made to make appropriate red phosphors. Currently most of the available red phosphors still have certain problems.[10,11] For example, oxide phosphors[12–16] cannot absorb blue light efficiently and sulfide phosphors[17–19] are unstable because of their high sensitivity to hydrolysis reactions. As for the nitride phosphors,[20–23] they have overlapping re-absorption with the yellow phosphor and the synthesis conditions are rigid. Hence, it is very urgent to find a new red phosphor that can efficiently absorb blue light and has small overlap with the emission of the YAG:Ce³⁺ phosphor. The Mn⁴⁺ doped fluoride red phosphors[24–30] have been widely investigated in recent years. Their main advantage is that they can absorb near ultraviolet and blue light to produce narrow-band red emission with broad prospects to be used for white LEDs.

Recently, the Mn⁴⁺-doped fluoride phosphors $A_2MF_6:Mn^{4+}$ (A = Na, K, Rb, Cs, (NH₄), M = Si, Ti, Ge, Sn, Zr)[31–38] and $BMF_6:Mn^{4+}$ (B = Ba, Zn, M = Si, Ti, Ge)[39–45] were reported. Some of them show high quantum efficiency, thermal stability against quenching and so on.[46] Recently, we had reported a red phosphor $K_2LiAlF_6:Mn^{4+}$,[47] which belongs to the elpasolite group of materials with a double perovskite structure. Though it has excellent thermal quenching behavior, the luminescence intensity is still not high enough. Therefore, it is an urgent task to improve its emission intensity to meet the requirements for various applications.

There are many reports[48,49] confirming that the Al³⁺ ions can be substituted by the Mn⁴⁺ ions as luminescent center because of similar effective ionic radius ($r = 0.53$ Å) when coordination number (CN) is six. Since both Al and Ga belong to the same IIIA group in the periodic table, it is believed that Al can be substituted by Ga to adjust the luminescence properties. Since the effective ionic radius of Ga³⁺ ($r = 0.62$ Å) is a little bigger than Mn⁴⁺ ($r = 0.53$ Å) at CN = 6, it is strongly expected that the Mn⁴⁺ ions substitute for the Ga³⁺ ions sites easier, compared to Al³⁺ ions. Moreover, there is no research on this material up to date, and this also prompts us to study it.

In this work, we successfully synthesized a $K_2LiGaF_6:Mn^{4+}$ phosphor *via* a facile cation exchange method. By optimizing the synthesis conditions, we obtain the best sample. The structure, morphology, composition and temperature-dependent photoluminescence (PL) properties were investigated in details. The PL spectra of both $K_2LiAlF_6:Mn^{4+}$ and $K_2LiGaF_6:Mn^{4+}$ phosphor were compared together to verify the effect on PL properties by changing luminescent center ions. Finally, we fabricated a white LED using a blue LED chip combined with a yellow phosphor and $K_2LiGaF_6:Mn^{4+}$ red phosphor.

School of Chemistry, Sun Yat-sen University, No. 135, Xingang Xi Road, Guangzhou, 510275, P. R. China. E-mail: ceswj@mail.sysu.edu.cn

College of Mathematics and Physics, Chongqing University of Posts and Telecommunications, 2 Chongwen Road, Nan'an District, Chongqing 400065, P. R. China

Institute of Physics, University of Tartu, W. Ostwald Str. 1, Tartu 50411, Estonia

Institute of Physics, Jan Dlugosz University, Armii Krajowej 13/15, PL-42-201, Czestochowa, Poland

2. Experimental

2.1 Preparation of K_2LiGaF_6

0.3447 g $LiNO_3$ and 1.0110 g KNO_3 were weighted and dissolved in 5 ml 1 mol L^{-1} $Ga(NO_3)_3$ solution. After stirring for 30 minutes, a transparent solution was obtained. HF (48%) solution was dropped slowly to the solution under stirring. A white precipitate K_2LiGaF_6 was obtained and washed with deionized water for several times and dried at 70 °C for 12 h.

2.2 Preparation of K_2LiGaF_6:Mn^{4+}

0.1344 g prepared K_2LiGaF_6 were weighted and added into 2 ml HF (48%) solution contained 0.0012 g K_2MnF_6. After stirring for 30 minutes, the suspension was centrifuged and washed with acetone for several times. The K_2LiGaF_6:Mn^{4+} phosphor was prepared after dried at 70 °C for 12 h.

2.3 Fabrication of WLEDs

WLEDs were fabricated by combining a blue LED chip (450–460 nm, 3.0–3.4 V, 350 mA), yellow phosphor YAG:Ce^{3+} and K_2LiGaF_6:Mn^{4+} red phosphor. The phosphors were mixed with silicone thoroughly and coated on the surface of the chip to produce WLEDs.

2.4 Characterization

XRD patterns were recorded using powder X-ray diffraction (XRD, Rigaku D/MAX 2200 VPC) with Cu Kα1 radiation (λ = 1.5405 Å) at a scanning rate of 10° min^{-1} over a 2θ range from 10° to 80°. The morphology of the as-prepared products was measured by SEM (FEI Quanta 400). Transmission electron microscopy (TEM), selected area electron diffraction (SAED) and elemental composition were obtained from an FEI Tecnai G2 Spirit. Photoluminescence excitation (PLE) and photoluminescence (PL) spectra were determined on an FSP920-combined time resolved and steady-state fluorescence spectrometer (Edinburgh Instruments) with a 450 W xenon lamp as the excitation source. Electron paramagnetic resonance (EPR) analyses were measured on spectrometer (BRÜCKNER A300-10-12) with frequency of 9.8 GHz and attenuator of 30 dB. The photoelectric properties of the white LED devices were measured by Labsphere LPS-100-0260 and Labsphere CDS2100.

3. Results and discussion

3.1 Phase, structure and spectroscopic studies

Fig. 1(a) shows the XRD patterns of K_2LiGaF_6 and K_2LiGaF_6:Mn^{4+}. The diffraction peaks of K_2LiGaF_6:Mn^{4+} can be indexed to the standard pattern of cubic phase K_2LiGaF_6 (PDF no. 22-1225) with a unit cell $a = b = c = 7.97$ Å, $\alpha = \beta = \gamma = 90°$ and the volume $V = 506.3$ Å^3. The main peaks located at 19.3°, 31.8° and 45.5°, corresponding to the (111), (220) and (400) reflections, respectively. The reaction can be expressed as follows:

$$LiNO_3 \text{ (aq.)} + 2KNO_3 \text{ (aq.)} + Ga(NO_3)_3 \text{ (aq.)}$$
$$+ 6HF \text{ (aq.)} == K_2LiGaF_6 \text{ (s)} + 6HNO_3 \text{ (aq.)}$$
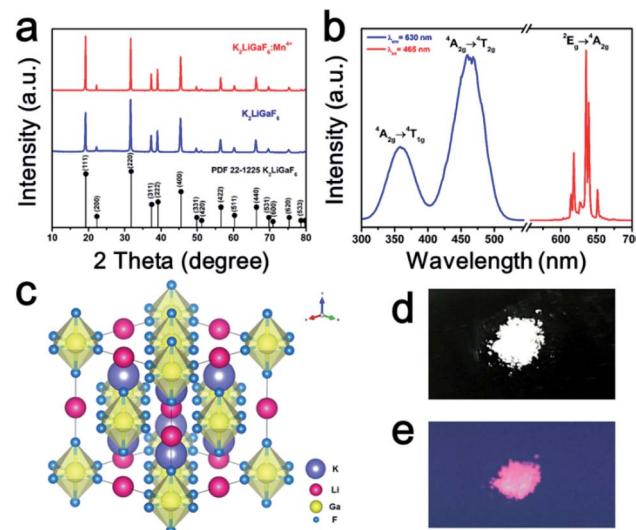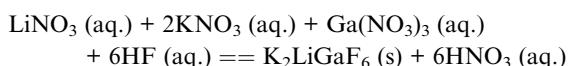

Fig. 1 (a) XRD patterns of K_2LiGaF_6 and K_2LiGaF_6:Mn^{4+}, (b) PLE and PL spectra of K_2LiGaF_6:Mn^{4+}, (c) structure diagram, (d) phosphor under natural light and (e) phosphor under UV-light.

When the nitrates are dissolved in the solution, the F^- anions bond the cations to form the K_2LiGaF_6 because of their strong ability of coordination. After the pure matrix phase is obtained, Mn^{4+} can be doped into it in the HF solution to form K_2LiGaF_6:Mn^{4+}. Fig. 1(b) exhibits the photoluminescence excitations (PLE) and PL spectra of K_2NaGaF_6:1% Mn^{4+}. The PLE spectra contain two bands from 300 nm to 500 nm, centered at ~360 nm and ~465 nm when monitored at 630 nm. These two excitation bands are due to the $^4A_{2g} \rightarrow {}^4T_{1g}$ and $^4A_{2g} \rightarrow {}^4T_{2g}$ spin-allowed transitions of Mn^{4+}. The phosphor emits a series of narrow band emission lines located at 610 nm, 614 nm, 623 nm, 632 nm, 636 nm and 649 nm, which are attributed to the spin-forbidden $^2E_g \rightarrow {}^4A_{2g}$ transitions of Mn^{4+} and its vibronic sidebands, under 465 nm excitation. According to the group theory, the octahedral symmetry O_h has six fundamental internal vibronic modes, namely, v_1 (A_{1g}), v_2 (E_g), v_3 (T_{1u}), v_4 (T_{1u}), v_5 (T_{2g}) and v_6 (T_{2u}).[46] The three peaks at longer than 623 nm wavelengths are ascribed to the Stokes v_6, v_4 and v_3 peaks, and the two other peaks at shorter than 623 nm are the anti-Stokes v_6 and v_4 peaks. The peak at 623 nm is the zero phonon line (ZPL), which is the electric dipole forbidden in the octahedral $[MnF_6]^{2-}$.[50] It has been reported that the ZPL emission intensity depends on the local symmetry of the Mn^{4+} ion. The higher the distortion of the octahedron, the stronger the ZPL emission intensity.[51] The structure scheme and coordination environment of K_2LiGaF_6 are shown in Fig. 1(c). The Ga^{3+} ions and Li^+ ions are surrounded by six F^- ions to form two types of octahedrons. The K^+ ions are at the center of a polyhedron formed by 12 neighbouring F^-. The $[GaF_6]^{3-}$ and $[LiF_6]^{3-}$ octahedrons share corners in a network. The Ga–F bond length is 1.8419 Å, and the Li–F bond length is 2.1431 Å, with bond angles $\angle FGaF = \angle FLiF = 90°$. Since the effective ionic radius of Mn^{4+} ($r = 0.53$ Å) at CN = 6 is close to Ga^{3+} ($r = 0.62$ Å), the Mn^{4+} ions substitute for the Ga^{3+} ions sites. Because of the ionic radii and valence state mismatch, the octahedrons distort

to some extent. The body color of phosphor is white under natural light and it emits red light under 365 nm UV-light, as shown in Fig. 1(d) and (e), respectively.

3.2 Morphology and composition analysis

Fig. 2(a) and (b) exhibit the SEM and TEM images of $K_2LiGaF_6:Mn^{4+}$. The SEM image shows that the as-synthesized sample consists of irregular aggregated particles with the size of about 100–200 nm. The particle mean diameter is 67 nm. This is different from other reported microscale Mn^{4+}-doped fluoride phosphors.[52–54] As shown in the inset of Fig. 2(b), the selected area electron diffraction (SAED) suggests that the samples are single crystals, of which the distinct diffraction dots can be indexed to the cubic phase K_2LiGaF_6. Fig. 2(c) shows the elemental composition analysis of $K_2LiGaF_6:Mn^{4+}$ sample, which were quantitatively carried out by using energy dispersive spectrometer (EDS) to further prove the purity of the as-synthesized sample. Li element is too light to be detected. It is clearly seen that K, Ga, F and Mn elements are included and for the reason of low Mn concentration, the Mn peaks are very weak. The atom percentages of K, Ga and F are about 21.5%, 11.6% and 52.8%, respectively, which is almost close to 2 : 1 : 6 ratio, *i.e.*, the stoichiometric atom ratio of K_2LiGaF_6. These results further indicate that the as-obtained phosphor is in a pure phase.

3.3 Room temperature PL properties

To optimize the luminescence performance of $K_2LiGaF_6:Mn^{4+}$, the effects of the nominal molar concentration of doped Mn^{4+}, reaction time and reaction temperature were systematically investigated, as shown in Fig. S1–S3 in ESI.† By adjusting the reaction conditions, the best sample $K_2LiGaF_6:1\% Mn^{4+}$ was
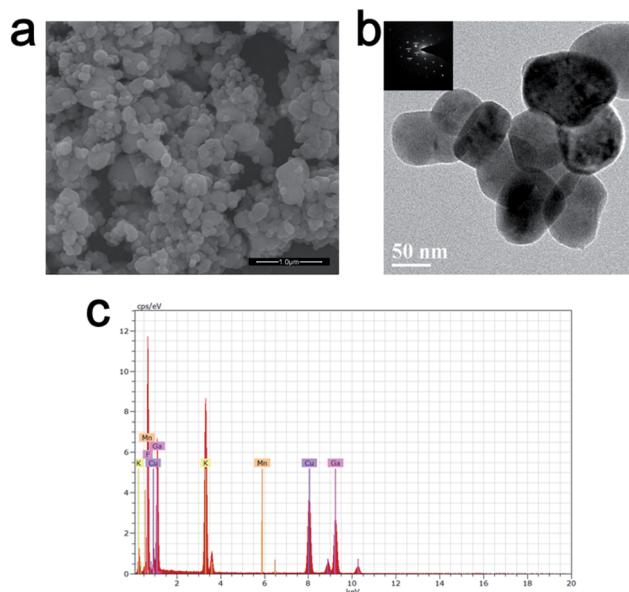
obtained under 20 °C for 1 h. In this way, the PL intensity can be increased 3.5 times.

The optimized phosphor shows much higher emission intensity than $K_2LiAlF_6:Mn^{4+}$ (Fig. 3). We attribute this result to the considerable ionic radii difference between Ga^{3+} and Al^{3+}. Since Ga^{3+} ($r = 0.62$ Å) is a little bigger than Al^{3+} ($r = 0.535$ Å), there is more space to be occupied by Mn^{4+} ($r = 0.53$ Å) at the Ga position. Such a large cavity – especially taken together with the difference of electric charges of Mn^{4+} and Ga^{3+} – would favour the off-center displacement of the Mn^{4+} ions. Such a displacement will lower the symmetry of the MnF_6 octahedra by eliminating the inversion center. As a result, the PL intensity of $K_2LiGaF_6:Mn^{4+}$ is much higher than that one of $K_2LiAlF_6:Mn^{4+}$. To further prove the concentration of Mn^{4+} is higher in K_2LiGaF_6, we measure the EPR spectra of two phosphors with the same doping concentration in Fig. 3(b). The signal of Mn^{4+} ions in K_2LiGaF_6 host is six featured peaks,[55] while it is much lower in K_2LiAlF_6. This indicates the concentration of Mn^{4+} ions is truly higher in K_2LiGaF_6 so that leads to higher emission intensity.

3.4 Temperature-dependent PL properties

The temperature-dependent emission spectra of $K_2LiGaF_6:Mn^{4+}$ in the 300–500 K temperature range under 465 nm excitation are presented in Fig. 4(a). Apparently, there is no shift or broadening of the emission peaks but the intensity decreases gradually with the increasing temperature. Fig. 4(b) reveals this trend clearly. It can be seen that the emission intensity is almost the same in the temperature range from 300 K to 375 K and then drops sharply with the temperature above 400 K. At 425 K (150 °C), it remains 88.8% of the initial intensity at 300 K. Similar thermal quenching behavior of Mn^{4+} ion in fluoride phosphors had been reported for several times.[49,56,57] We determine the activation energy (E_a) of $K_2LiGaF_6:Mn^{4+}$ for thermal quenching using eqn (1).[58]

$$I_T = \frac{I_0}{1 + A \exp\left(-\dfrac{E_a}{k_B T}\right)} \quad (1)$$

where I_0 is the initial emission intensity, I_T is the intensity at different temperatures, E_a is activation energy of thermal quenching, A is a constant, and k_B is the Boltzmann constant (8.617×10^{-5} eV K^{-1}). Its value for $K_2LiGaF_6:Mn^{4+}$ is about 0.24 eV, which is close to other fluoride phosphors we had

**Fig. 2** (a) SEM and (b) TEM (the inset is SAED patterns of one particle) images and (c) quantitative elemental composition data of $K_2LiGaF_6:Mn^{4+}$.
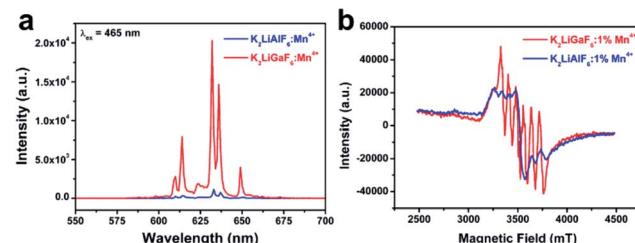

**Fig. 3** (a) PL spectra and (b) EPR spectra of $K_2LiAlF_6:Mn^{4+}$ and $K_2LiGaF_6:Mn^{4+}$.
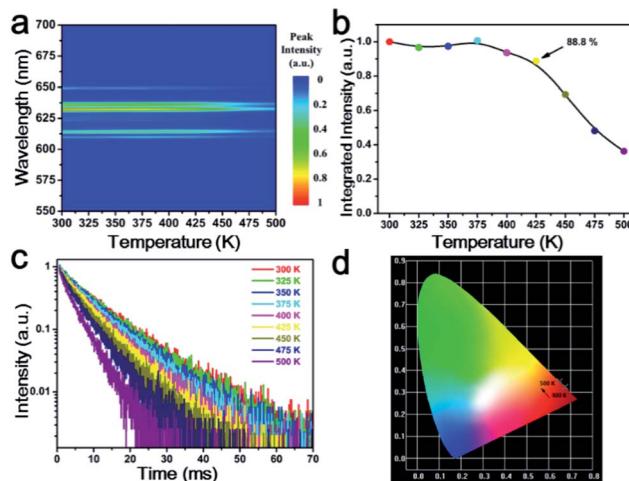
Fig. 4 (a) Temperature-dependent emission spectra of K_2LiGaF_6:Mn^{4+} from 300 K to 500 K, (b) PL integrated intensity, (c) decay time and (d) CIE chromaticity coordinates of K_2LiGaF_6:Mn^{4+} from 300 K to 500 K.

reported before.[47] The decay time of K_2LiGaF_6:Mn^{4+} in Fig. 4(c) shows that the luminescence intensity undergoes a rapid decrease from 300 K to 500 K, which is due to the increase in the non-radiative transition probability at higher temperature.[59] Therefore, the decay time becomes shorter with the increasing temperature. The CIE color coordinates of K_2LiGaF_6:Mn^{4+} change from (0.675, 0.325) to (0.651, 0.349) in the whole temperature range of 300–500 K (Fig. 4(d)). More CIE values can be found in Table S1 in ESI.† Obviously, K_2LiGaF_6:Mn^{4+} shows small shift of color coordinates in the red region, which is mainly due to the tiny shift and broadening of sharp red emission peaks of Mn^{4+}. This further suggests that K_2LiGaF_6:Mn^{4+} shows excellent color stability. Moreover, the color purity of K_2LiGaF_6:Mn^{4+} calculated by eqn (2)[60] is about 94%.

$$\text{Color purity} = \frac{\sqrt{(x - x_i)^2 + (y - y_i)^2}}{\sqrt{(x_d - x_i)^2 + (y_d - y_i)^2}} \quad (2)$$

where (x, y) is the color coordinates of the phosphor, (x_i, y_i) is the CIE of an equal-energy illuminant with a value of (0.3333, 0.3333), and (x_d, y_d) is the chromaticity coordinates corresponding to the dominant wavelength of the light source.

3.5 LED application

Fig. 5(a) shows the current-dependent LED performance fabricated with a blue LED chip combined with the YAG:Ce^{3+} and K_2LiGaF_6:Mn^{4+} phosphors. The sharp peak located at about 450 nm belongs to blue LED chip and the broad band centered at 560 nm is attributed to YAG:Ce^{3+}. Narrow peaks around 630 nm are the emission lines of K_2LiGaF_6:Mn^{4+}. The intensity grows with the increasing drive current. The band shapes and positions of emission peaks exhibit no remarkable change, revealing good stabilities both in color and CCT of this LED. Fig. 5(b) shows the CIE coordinate diagram of the white LED with the color point lying on the black body locus under various
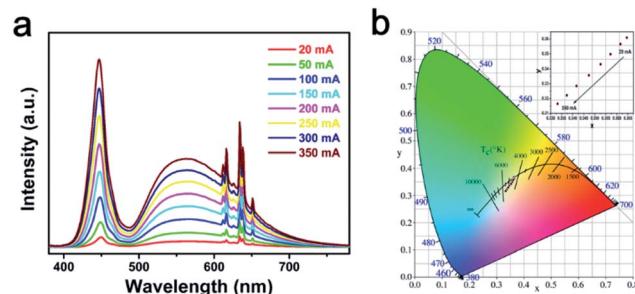
Fig. 5 (a) Electroluminescence spectra and (b) CIE chromaticity diagram of fabricated white LED under various drive currents.

drive currents. The chromaticity coordinates of them are marked in CIE 1931 color spaces and they are almost laid on the black body locus. All important photoelectric parameters for clarity are presented in Table S2.† Slight variations of the color rendering index (Ra) and chromaticity coordinates are observed during the drive current range. With increasing drive current from 20 to 350 mA, the luminous efficacy (LE) gradually decreases from 53.3 to 40.7 lm W^{-1}, due to the monotonously decreased external quantum efficiency of the blue InGaN chip and the low quantum efficiency of K_2LiGaF_6:Mn^{4+}. Commercial white LEDs only using a single YAG:Ce^{3+} phosphor has a low CRI,[61] typically, Ra < 70. By adding K_2LiGaF_6:Mn^{4+} red phosphors, CRI is improved to 80.8. Specifically, all the R9 values are positive, which suggests good rendition of the red component.

4. Conclusions

In summary, a novel red emitting K_2LiGaF_6:Mn^{4+} phosphor was synthesized by a facile cation exchange method. It exhibits a broadband excitation extending from 300 to 500 nm and an ideal narrow band emission centered at 632 nm, which matches well with the UV and blue LED chips. The PL properties of the phosphors were optimized by varying the Mn^{4+} concentration, reaction times, and reaction temperature. For changing the luminescent center ions, the emission intensity of K_2LiGaF_6:Mn^{4+} is much higher than K_2LiAlF_6:Mn^{4+}. It is a good way to adjust PL properties of luminescent materials. Moreover, K_2LiGaF_6:Mn^{4+} exhibits an excellent thermal quenching behavior and color stability over the temperature range of 300–500 K. The Ra, CCT and luminous efficiency of fabricated WLED are 79.5, 4363 K and 53.3 lm W^{-1}, respectively. All these results imply that the K_2LiGaF_6:Mn^{4+} red emitting phosphor has potential applications in white LEDs.

Acknowledgements

References

1 E. F. Schubert, T. Gessmann and J. K. Kim, *Light emitting diodes*, Wiley Online Library, 2005.

2 S. Pimputkar, J. S. Speck, S. P. DenBaars and S. Nakamura, *Nat. Photonics*, 2009, **3**, 180–182.

3 H. A. Höppe, *Angew. Chem., Int. Ed.*, 2009, **48**, 3572–3582.

4 C. Feldmann, T. Jüstel, C. R. Ronda and P. J. Schmidt, *Adv. Funct. Mater.*, 2003, **13**, 511–516.

5 J. He, Y. He, Y. Chen, B. Lei, H. Zhang, J. Zhuang, M. Zheng and Y. Liu, *RSC Adv.*, 2016, **6**, 104724–104730.

6 C. Zhao, Z. Xia and M. Li, *RSC Adv.*, 2014, **4**, 33114–33119.

7 S. Ye, F. Xiao, Y. X. Pan, Y. Y. Ma and Q. Y. Zhang, *Mater. Sci. Eng., R*, 2010, **71**, 1–34.

8 E. F. Schubert and J. K. Kim, *Science*, 2005, **308**, 1274–1278.

9 C. C. Lin and R.-S. Liu, *J. Phys. Chem. Lett.*, 2011, **2**, 1268–1277.

10 C. C. Lin, A. Meijerink and R. S. Liu, *J. Phys. Chem. Lett.*, 2016, **7**, 495–503.

11 T. Wang and H. Li, *Chem.–Eur. J.*, 2016, **22**, 12400–12405.

12 J. Liu, B. Xu, C. Song, H. Luo, X. Zou, L. Han and X. Yu, *CrystEngComm*, 2012, **14**, 2936–2943.

13 Y. Chen, J. Wang, C. Liu, X. Kuang and Q. Su, *Appl. Phys. Lett.*, 2011, **98**, 081917.

14 O. Milosevic, L. Mancic, M. E. Rabanal, J. M. Torralba, B. Yang and P. Townsend, *J. Electrochem. Soc.*, 2005, **152**, G707–G713.

15 J.-G. Li, X. Li, X. Sun and I. Takamasa, *J. Phys. Chem. C*, 2008, **112**, 11707–11716.

16 M. Peng, X. Yin, P. A. Tanner, M. G. Brik and P. Li, *Chem. Mater.*, 2015, **27**, 2938–2945.

17 Y. Li, D. Dai and S. Cai, *J. Chin. Rare Earth Soc.*, 1996, **14**, 16–19.

18 G. A. Kumar, D. X. Liu, Y. Tian, M. G. Brik and D. K. Sardar, *Opt. Mater.*, 2015, **50**, 199–203.

19 C. Guo, D. Huang and Q. Su, *Mater. Sci. Eng., B*, 2006, **130**, 189–193.

20 R.-J. Xie, N. Hirosaki, K. Sakuma, Y. Yamamoto and M. Mitomo, *Appl. Phys. Lett.*, 2004, **84**, 5404–5406.

21 X. Piao, K.-i. Machida, T. Horikawa, H. Hanzawa, Y. Shimomura and N. Kijima, *Chem. Mater.*, 2007, **19**, 4592–4599.

22 T.-C. Liu, B.-M. Cheng, S.-F. Hu and R.-S. Liu, *Chem. Mater.*, 2011, **23**, 3698–3705.

23 Y. Q. Li, N. Hirosaki, R. J. Xie, T. Takeda and M. Mitomo, *Chem. Mater.*, 2008, **20**, 6704–6714.

24 M.-H. Du, *J. Mater. Chem. C*, 2014, **2**, 2475–2481.

25 M. Brik, S. Camardello and A. Srivastava, *ECS J. Solid State Sci. Technol.*, 2015, **4**, R39–R43.

26 M. H. Du, *J. Lumin.*, 2015, **157**, 69–73.

27 H.-D. Nguyen and R.-S. Liu, *J. Mater. Chem. C*, 2016, **4**, 10759–10775.

28 M. G. Brik and A. M. Srivastava, *J. Lumin.*, 2013, **133**, 69–72.

29 Z. Zhou, N. Zhou, M. Xia, M. Yokoyama and H. T. Hintzen, *J. Mater. Chem. C*, 2016, **4**, 9143–9161.

30 D. Chen, Y. Zhou and J. Zhong, *RSC Adv.*, 2016, **6**, 86285–86296.

31 S. Adachi and T. Takahashi, *J. Appl. Phys.*, 2008, **104**, 023512.

32 T. Takahashi and S. Adachi, *J. Electrochem. Soc.*, 2008, **155**, E183–E188.

33 Y. Arai and S. Adachi, *J. Lumin.*, 2011, **131**, 2652–2660.

34 Z. Wang, Y. Liu, Y. Zhou, Q. Zhou, H. Tan, Q. Zhang and J. Peng, *RSC Adv.*, 2015, **5**, 58136–58140.

35 Z. Wang, Y. Zhou, Y. Liu, Q. Zhou, L. Luo, H. Tan, Q. Zhang, G. Chen and J. Peng, *RSC Adv.*, 2015, **5**, 82409–82414.

36 M. Takarkhede, R. R. Patil and S. V. Moharil, *Study of photoluminescence in $ABSiF_6:Mn^{4+}$ (A=K, B=Na, Cs) phosphor*, AIP Publishing, 2016, vol. 1728, p. 020441.

37 L. Xi, Y. Pan, S. Huang and G. Liu, *RSC Adv.*, 2016, **6**, 76251–76258.

38 W.-L. Wu, M.-H. Fang, W. Zhou, T. Lesniewski, S. Mahlik, M. Grinberg, M. G. Brik, H.-S. Sheu, B.-M. Cheng, J. Wang and R.-S. Liu, *Chem. Mater.*, 2017, **29**, 935–939.

39 X. Jiang, Z. Chen, S. Huang, J. Wang and Y. Pan, *Dalton Trans.*, 2014, **43**, 9414–9418.

40 Q. Zhou, Y. Zhou, Y. Liu, L. Luo, Z. Wang, J. Peng, J. Yan and M. Wu, *J. Mater. Chem. C*, 2015, **3**, 3055–3059.

41 X. Gao, Y. Song, G. Liu, X. Dong, J. Wang and W. Yu, *Dalton Trans.*, 2016, **45**, 17886–17895.

42 R. Hoshino, T. Nakamura and S. Adachi, *ECS J. Solid State Sci. Technol.*, 2016, **5**, R37–R43.

43 Y. Pan, Z. Chen, X. Jiang, S. Huang, M. Wu and A. Srivastava, *J. Am. Ceram. Soc.*, 2016, **99**, 3008–3014.

44 Y. Zhou, Q. Zhou, Y. Liu, Z. Wang, H. Yang and Q. Wang, *Mater. Res. Bull.*, 2016, **73**, 14–20.

45 G. Mo, W. Wang, K. Wang, G. Wen, M. Zhu and J. Wang, *J. Mater. Sci.*, 2017, **28**, 8155–8159.

46 H. Zhu, C. C. Lin, W. Luo, S. Shu, Z. Liu, Y. Liu, J. Kong, E. Ma, Y. Cao, R. S. Liu and X. Chen, *Nat. Commun.*, 2014, **5**, 4312.

47 Y. Zhu, L. Huang, R. Zou, J. Zhang, J. Yu, M. Wu, J. Wang and Q. Su, *J. Mater. Chem. C*, 2016, **4**, 5690–5695.

48 L. Chen, X. Deng, E. Zhao, X. Chen, S. Xue, W. Zhang, S. Chen, Z. Zhao, W. Zhang and T.-S. Chan, *J. Alloys Compd.*, 2014, **613**, 312–316.

49 E. Song, J. Wang, J. Shi, T. Deng, S. Ye, M. Peng, J. Wang, L. Wondraczek and Q. Zhang, *ACS Appl. Mater. Interfaces*, 2017, **9**, 8805–8812.

50 Y. Jin, M. H. Fang, M. Grinberg, S. Mahlik, T. Lesniewski, M. G. Brik, G. Y. Luo, J. G. Lin and R. S. Liu, *ACS Appl. Mater. Interfaces*, 2016, **8**, 11194–11203.

51 L. L. Wei, C. C. Lin, Y. Y. Wang, M. H. Fang, H. Jiao and R. S. Liu, *ACS Appl. Mater. Interfaces*, 2015, **7**, 10656–10659.

52 Y. K. Xu and S. Adachi, *J. Appl. Phys.*, 2009, **105**, 013525.

53 Y. K. Xu and S. Adachi, *J. Electrochem. Soc.*, 2011, **159**, E11–E17.

54 C. Liao, R. Cao, Z. Ma, Y. Li, G. Dong, K. N. Sharafudeen, J. Qiu and J. Heo, *J. Am. Ceram. Soc.*, 2013, **96**, 3552–3556.

55 Y. Li, Y.-Y. Li, K. Sharafudeen, G.-P. Dong, S.-F. Zhou, Z.-J. Ma, M.-Y. Peng and J.-R. Qiu, *J. Mater. Chem. C*, 2014, **2**, 2019–2027.

56 L. Huang, Y. Zhu, X. Zhang, R. Zou, F. Pan, J. Wang and M. Wu, *Chem. Mater.*, 2016, **28**, 1495–1502.

57 T. T. Deng, E. H. Song, J. Sun, L. Y. Wang, Y. Deng, S. Ye, J. Wang and Q. Y. Zhang, *J. Mater. Chem. C*, 2017, **5**, 2910–2918.

58 X. Zhang, J. Wang, L. Huang, F. Pan, Y. Chen, B. Lei, M. Peng and M. Wu, *ACS Appl. Mater. Interfaces*, 2015, **7**, 10044–10054.

59 R. Shi, J. Xu, G. Liu, X. Zhang, W. Zhou, F. Pan, Y. Huang, Y. Tao and H. Liang, *J. Phys. Chem. C*, 2016, **120**, 4529–4537.

60 X. Zhang, Y. T. Tsai, S. M. Wu, Y. C. Lin, J. F. Lee, H. S. Sheu, B. M. Cheng and R. S. Liu, *ACS Appl. Mater. Interfaces*, 2016, **8**, 19612–19617.

61 A. Birkel, K. A. Denault, N. C. George, C. E. Doll, B. Héry, A. A. Mikhailovsky, C. S. Birkel, B.-C. Hong and R. Seshadri, *Chem. Mater.*, 2012, **24**, 1198–1204.